Journal of Alloys and Compounds 509 (2011) 8176–8182

Contents lists available at ScienceDirect

Journal of Alloys and Compounds

journal homepage: www.elsevier.com/locate/jallcom

Solid/liquid interaction between a multicomponent FeCrNiCoMnAl high entropy alloy and molten aluminum

Hung-Hua Yang[a], Wen-Ta Tsai[a,*], Jui-Chao Kuo[a], Chih-Chao Yang[b]

[a] Department of Materials Science and Engineering, National Cheng Kung University, 1 Ta-Hsueh Road, Tainan 701, Taiwan
[b] Industrial Technology Research Institute, 31 Gongye 2nd Rd., Annan District, Tainan 709, Taiwan

ARTICLE INFO

Article history:
Received 16 March 2011
Received in revised form 24 May 2011
Accepted 26 May 2011
Available online 6 June 2011

Keywords:
Multicomponent high-entropy alloy
Molten aluminum
Interfacial reaction
Electron back scattering diffraction

ABSTRACT

This study investigates the interfacial reaction between an as-cast multicomponent FeCrNiCoMnAl high-entropy alloy (HEA) and an Al melt at 700 ° C. The microstructure, phase identification, and chemical composition were analyzed by using scanning electron microscopy (SEM), energy dispersive spectroscopy (EDS), X-ray diffraction (XRD), transmission electron microscopy (TEM) and electron back scattering diffraction (EBSD). The results showed that the contact between the solid substrate and the Al melt resulted in the formation of a region with complicated microstructure at the interface. The dissolution of the substrate alloying elements into the Al melt also caused chemical composition and phase changes in the solidified Al crust.

1. Introduction

Molds or crucibles made of metallic materials are sometimes used to handle liquid melts, especially those with low melting points, in hot dipping and casting processes [1–3]. For aluminum casting or die-casting, iron-based alloys are the most commonly used molding materials. However, aluminum melt is very corrosive and can react with iron to form intermetallics when they come into contact with each other [4,5]. To extend the service life of metallic molds that deal with aluminum melts, other materials are always used as substitutes for iron-based alloys. Since chemical stability and adequate mechanical strength are crucial to increasing the service life of metallic molds acting as containers for liquid metal, the substituting alloy should have the proper chemical composition and microstructure to provide corrosion resistance and high temperature strength.

Newly established multi-components or high entropy alloys (HEA) [6–8] containing transition metal elements have been reported exhibiting high strength, resistance to wear, thermal stability, and oxidation resistance at high temperatures [9–14]. In the study of TiCoCrFeNiCuAl high entropy alloy, Zhang et al. [14] reported that this material exhibited high fracture strength at high temperature, but its phase stability was affected by the alloying of Al. Therefore, the potential of HEAs for use as the crucible materials for aluminum melts is of interest. This study investigates the stability of an Al containing HEA in a pure aluminum melt at 700 °C. The HEA used in this study contained an almost equi-atomic ratio of Fe, Co, Ni, Cr, and Mn with 6.78 at% Al. We examine the resulting chemical composition and microstructural changes occurring in the substrate, the solidified melt and at the HEA/Al melt interface.

2. Experimental procedure

The FeCoNiCrMnAl high-entropy alloy with the chemical composition listed in Table 1 was prepared by vacuum induction melting. It was then casted into a mold with dimensions of 150 × 100 × 20 mm. After removing the surface scale, the ingot was then ground and cut into pieces, each with dimensions of 10 × 10 × 10 mm, for subsequent material characterization and hot dipping tests.

The hot dipping test was conducted in pure Al melt at 700 °C. The melt was prepared by loading a fixed amount (ca. 265 g) of Al block into a crucible made of alumina, which was then heated in a box furnace until the Al block fully melted and remained at 700 °C. Then, the HEA specimen was dipped into the melt for 20 s, 10 min and 1 h, respectively. After being removed from the melt and cooled, the hot-dipped HEA was cut in the middle for subsequent analyses.

The microstructures of the HEAs, before and after hot dipping in Al melt, were examined using an optical microscope and a scanning electron microscope (SEM). The specimens were first ground with SiC papers to a grit of #2000, followed by polishing in slurry containing Al_2O_3 powers with an average particle size of 0.3 μm. The polished specimen was then etched in the aqua regia (25 mL HNO_3 + 75 mL HCl) before microstructural examinations. The chemical compositions of the constituent phases in the substrate, the interfacial zone and the solidified Al melt were analyzed using an energy dispersive spectrometer (EDS) attached to SEM before and after hot dipping. Electron backscatter diffraction (EBSD) using the Kikuchi pattern (the Kikuchi bands were detected by TexSEM Laboratories (TSL) OIM analysis software) was employed to determine the crystal structure and phase change at the Al/HEA interface. The reaction product which formed immediately adjacent

* Corresponding author.
E-mail address: wttsai@mail.ncku.edu.tw (W.-T. Tsai).

0925-8388/$ – see front matter © 2011 Elsevier B.V. All rights reserved.
doi:10.1016/j.jallcom.2011.05.104

Table 1
Chemical composition of the FeCrNiCoMnAl high entropy alloy (HEA).

Element	Fe	Cr	Ni	Co	Mn	Al
Composition (wt.%)	19.02	16.85	20.60	19.20	17.55	6.78

to the HEA substrate was also analyzed using transmission electron microscopy (TEM).

3. Results and discussion

The cross-section images of the HEA after being immersed in the 700 °C Al melt for different periods of time were examined either using a digital camera or an SEM. Fig. 1(a) demonstrates the macroscopic cross-section view of a specimen fully immersed in the melt for 1 h. As revealed in this digital photo, the bright region in the center is the HEA surrounded by the solidified Al melt with a grey color and irregular shape. The fact that the initially straight edges of the HEA become slightly curved after hot dipping indicates the occurrence of solid/liquid interfacial reaction. The reaction between the HEA and the Al melt is further confirmed by the SEM back scattering electron (BSE) image of a specimen which was partially immersed in the Al melt for 1 h, as shown in Fig. 1(b). As indicated in this micrograph, a reaction zone can be clearly observed below the immersion line.

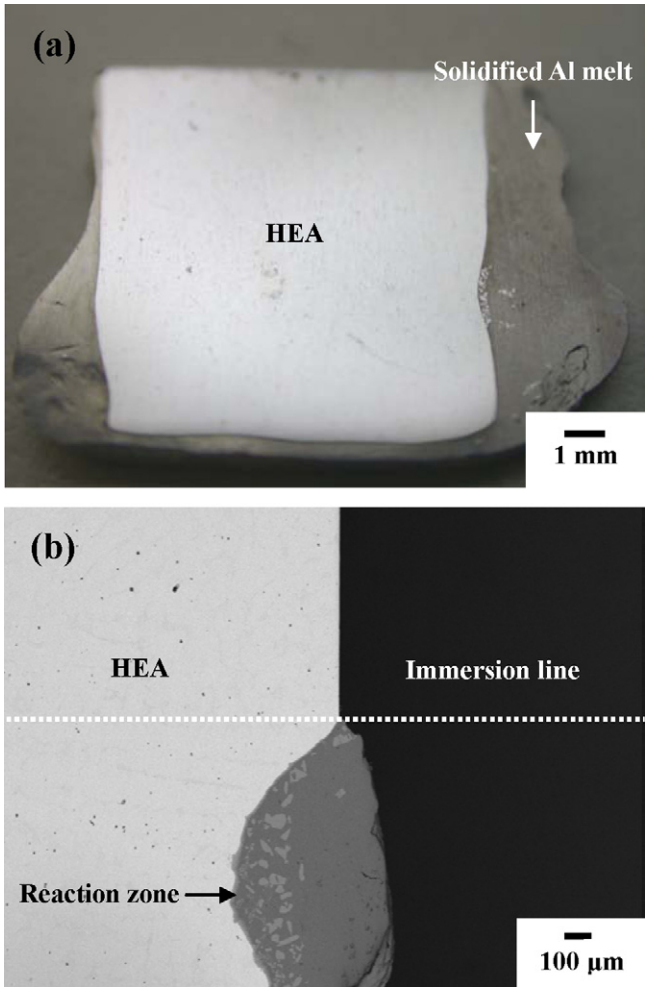

Fig. 1. Cross-section image of an HEA after immersion in 700 °C Al melt for 1 h, (a) digital microscope image for fully immersed specimen and (b) BSE image for partial immersed specimen.

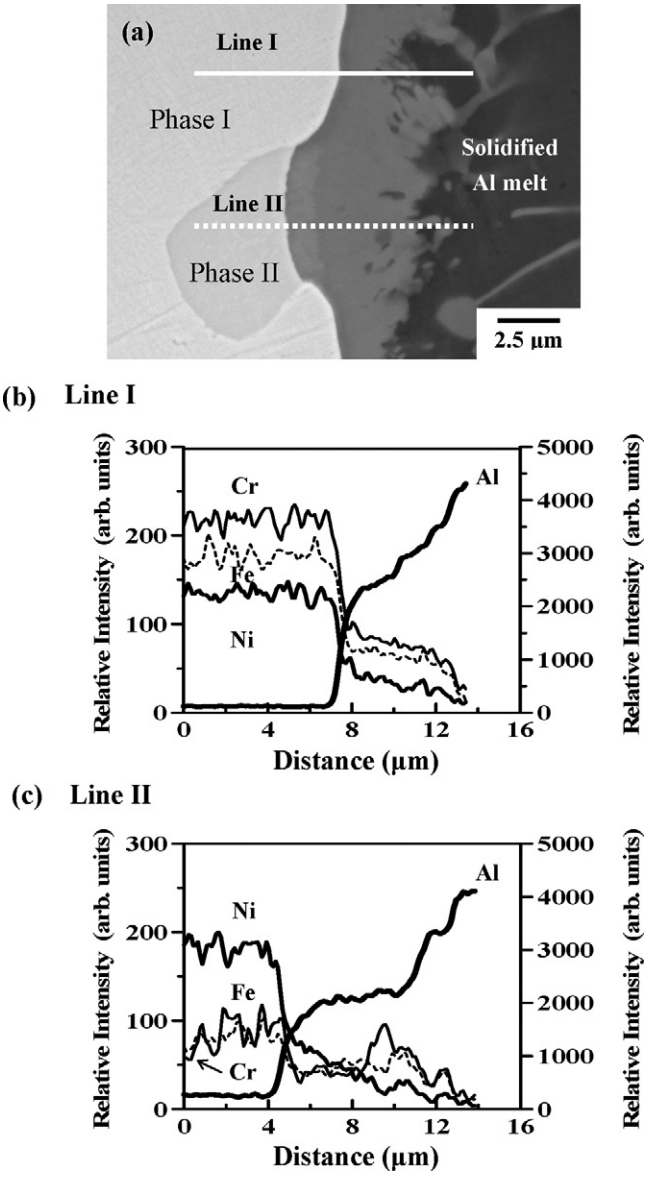

Fig. 2. (a) Cross-section SEM image exhibiting dual phase microstructure at the Al/HEA interface after immersion in 700 °C Al melt for 1 h, (b) the corresponding EDS line scan profile of phase I in (a), and (c) the corresponding EDS line scan profile of phase II in (a).

3.1. Solid/liquid reaction

After hot dipping in 700 °C Al melt for 1 h, the cross-section SEM micrograph showing the image at the interface is manifested in Fig. 2(a). To the left of this micrograph, the duplex microstructure containing phase I and II in the HEA is clearly revealed. At the far right of this micrograph, the dark region is the solidified Al layer. In between the HEA and the outer Al layer, immediately adjacent to the HEA surface, a grey region resulting from the solid/liquid reaction is displayed. The concentration changes of Fe, Cr, Ni and Al across the two dashed lines marked in Fig. 2(a) are shown in Fig. 2(b) and (c), respectively. The results of the EDS line scan across line I are manifested in Fig. 2(b). As can be seen from this figure, phase I in the HEA has higher Cr and Fe contents than Ni and Al contents. At the region about 1 um to the right of phase I, the Al content was higher than that in the bulk, indicating the inward diffusion of Al into the HEA. The grey region resulting from the solid/liquid reaction, to the right of the reaction interface, consists of noticeable amounts of Cr,

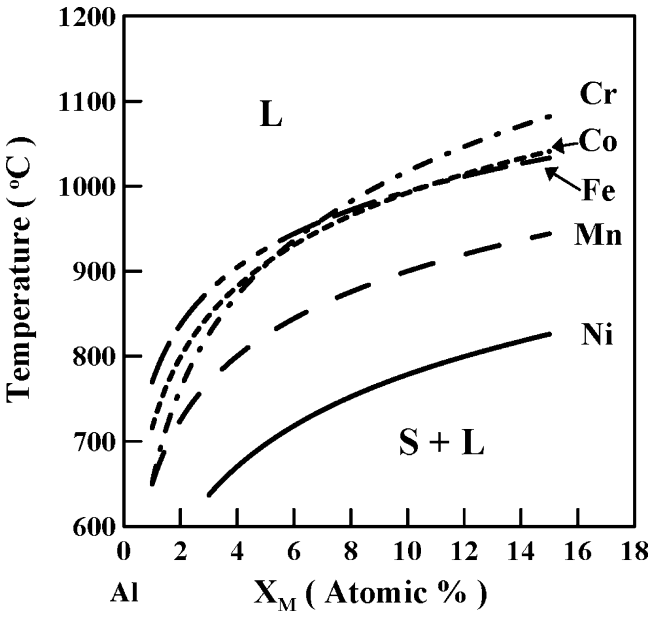

Fig. 3. Schematic diagram of the liquidus curves of the five Al–M systems.

Fe, and Ni, which decrease with increasing distance from the HEA surface. Similar results of the EDS scan across line II are displayed in Fig. 2(c). The formation of a thick layer of solid/liquid reaction product, in comparison with the thin Al-enriched surface layer formed in the phase I or II substrates, suggests that the dissolution of the HEA alloying elements into the Al liquid phase is more pronounced as compared with the counter-flux of Al into the HEA substrate. The more detail reactions occurred at the interface will be discussed in the following section.

It is noted from the micrograph shown in Fig. 2(a) that retreats of the surface at phase II with respect to phase I occurs, indicating a fast reaction between phase II/Al as compared with that at phase I/Al interface. More specifically, the dissolution of phase II into molten Al liquid is faster than that of phase I. Examination of the binary phase diagrams of the Al–M (M = Mn, Fe, Co and Ni) systems shows that each of these systems exhibits eutectic behavior in the Al-side, while the behavior of the Al–Cr system is peritectic [15]. It is also found that the liquidus temperature of the hypereutectic solid phase of the Al–Ni system is the lowest when compared with those of Al–Fe, Al–Cr, Al–Co, and Al–Mn systems. The comparison of the liquidus curves of the five Al–M systems is summarized in Fig. 3. As can be seen from this figure, the liquidus temperature of the Al-rich hypereutectic solid solution phase of the Al–Ni system is much lower than those containing Cr, Fe, Co and Mn. When solid HEA is in contact with Al melt, the dissolution of Al into both phases I and II in the HEA causes changes in melting point for both phases, each having different Al solubility. Since the Ni content in the phase II is higher (Fig. 2(c)), the dissolution of Al into the HEA, especially at the intimate contact interface, can more easily cause a lowering of the melting point in phase II than in phase I. This may explain the higher rate of retreat in the solid phase at the II/Al interface.

The microstructure of the solid/liquid reaction products formed near the interface is further examined by SEM under high magnification. Fig. 4 shows the cross-section BSE images for the specimens with hot dipping times of 20 s, 10 min, and 1 h, respectively. With a short (20 s) hot dipping, a discontinuous reaction occurred at the interface, as shown in Fig. 4(a). A thin layer of reaction product (marked as nanocrystalline phase layer, NPL), about 2–3 μm thick, was formed on top of the HEA. In this layer, nanocrystalline phases were identified by TEM and EBSD as will be discussed latter. EDS analysis indicates that this layer has a uniform chemical composition. The dark region to the right of the uniform reaction product layer is the solidified Al layer. Interestingly, large white particles are found present in the solidified Al matrix, as revealed in Fig. 4(a). These white particles are Al alloys containing a higher content of Cr, which have been confirmed as $Al_{13}Cr_2$ by using EDS and EBSD. Far away from the initial solid/liquid interface, a new phase (bright area marked as III_1) is seen dispersed in the solidified Al matrix. EDS

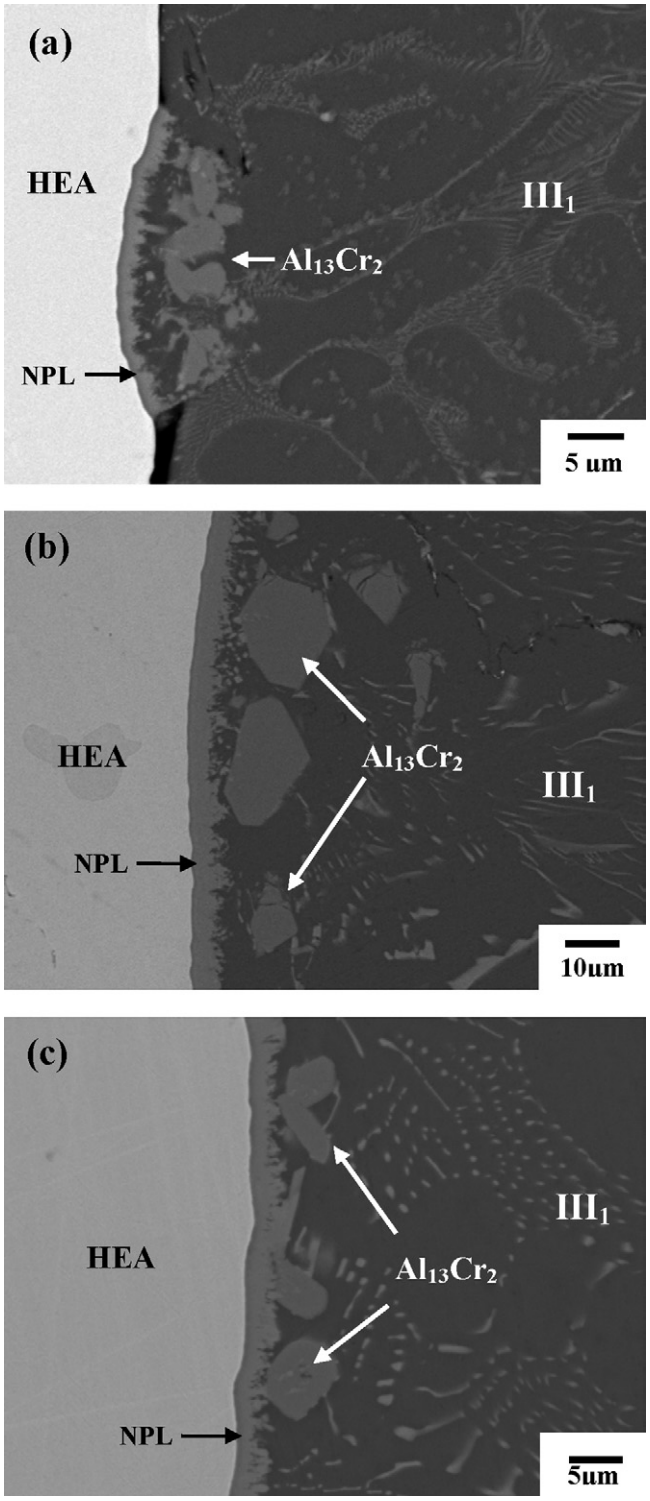

Fig. 4. Magnified cross-section BSE images of an HEA after immersion in 700 °C Al melt for (a) 20 s, (b) 10 min and (c) 1 h, showing the formation of a nanocrystalline phase layer (NPL), and precipitation of $Al_{13}Cr_2$ and III_1.

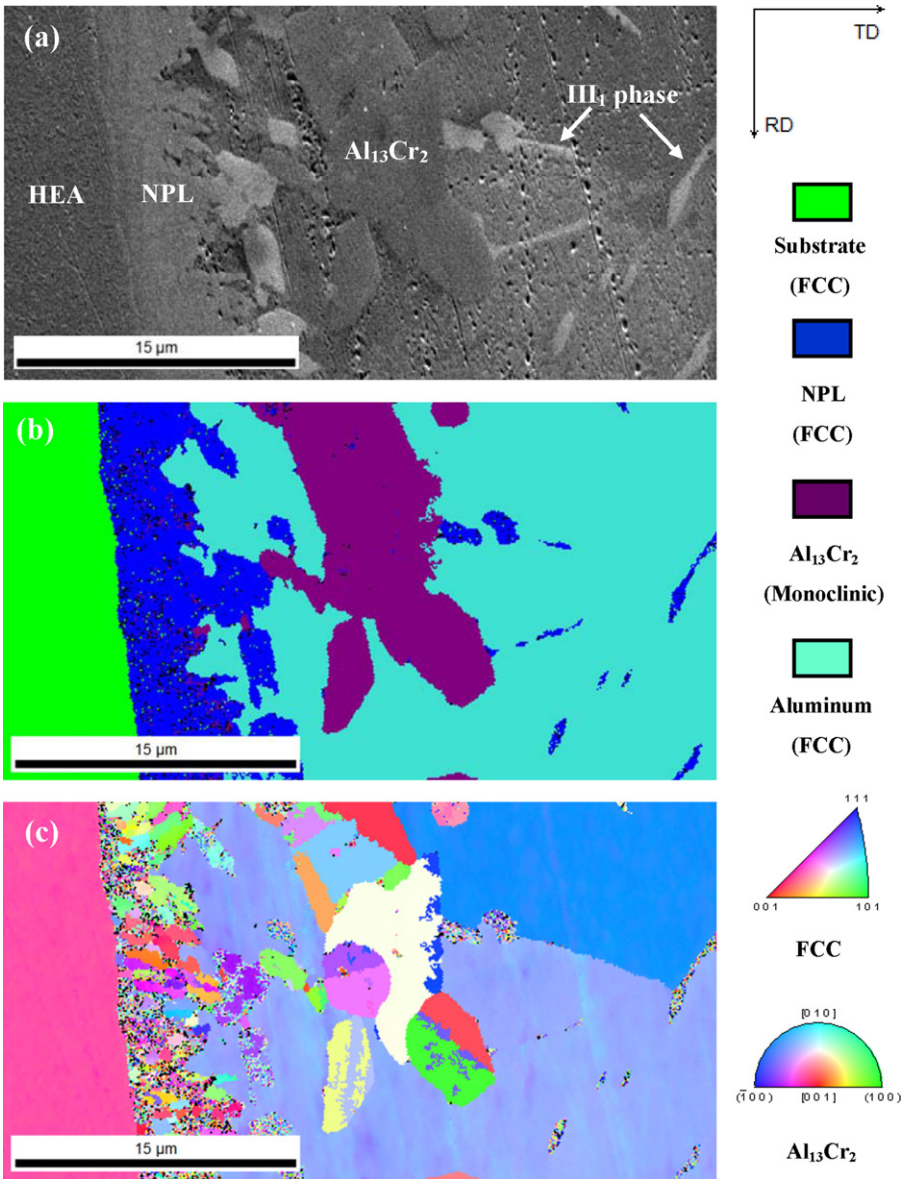

Fig. 5. (a) Cross-section SEM image of the Al/HEA interface, (b) phase map of the Al/HEA interface obtained from EBSD, the corresponding color (substrate in green, NPL in blue, $Al_{13}Cr_2$ phase in purple and aluminum phase in turquoise) coding for the phase map, and (c) the corresponding orientation maps assign as above mentioned structure. (For interpretation of the references to color in this figure legend, the reader is referred to the web version of the article.)

analysis indicates that the chemical composition of the dispersed phase mainly consists of Al with a relatively high concentration of Fe, Co and Ni which are dissolved from the HEA into the Al melt during hot dipping. After extending the dipping time to 10 min and 1 h, the SEM cross-section micrographs are shown in Fig. 4(b) and (c), respectively. Complete wetting results in the formation of a continuous reaction zone are shown in these figures. The microstructure is similar to that shown in Fig. 4(a).

The phase changes and reaction products formed in the solid/liquid interface are further examined using EBSD. Fig. 5 gives an example showing the EBSD results obtained for the HEA/Al interface with hot dipping for 1 h. The cross-section SEM image is shown in Fig. 5(a), while the phase map and orientation map obtained from the EBSD analysis of this area are displayed in Figs. 5(b) and (c), respectively. The phase map shown in Fig. 5(b) reveals two face-centered cubic (FCC) phases with different chemical composition (using simultaneous EBSD-EDS measurement), displayed in green and blue respectively. An $Al_{13}Cr_2$ phase in purple and an aluminum phase in turquoise color are also shown in this figure. The blue color region corresponds to the NPL layer. Some tiny black, purple and green spots are found dispersed within it. The black spots shown in the phase map represents that there is no Kikuchi pattern signal in the selected area, indicating the presence of an amorphous or nanocrystalline phase. The presence of purple spots indicates the precipitation of $Al_{13}Cr_2$ occurring in the NPL layer. The green spots represents the tiny FCC phase with (1 1 2) orientation. The origin of the fine green phase in the NPL layer needs further investigation. The EBSD result shown in Fig. 5(b) indicates that the substrate selected for analysis is exclusively phase I with FCC structure. The orientation map shown in Fig. 5(c) corresponds to that from the transverse direction (TD), which is normal to the HEA/Al interface. The microstructure with fine grain size feature in the NPL layer can also be seen in Fig. 5(c).

Since the crystallinity of the NPL layer cannot be adequately identified by EBSD as described above, TEM examination was performed. The TEM dark field image of a thin foil carefully taken from the NPL layer is shown in Fig. 6(a), and the corresponding selected area diffraction (SAD) pattern is displayed in Fig. 6(b). The

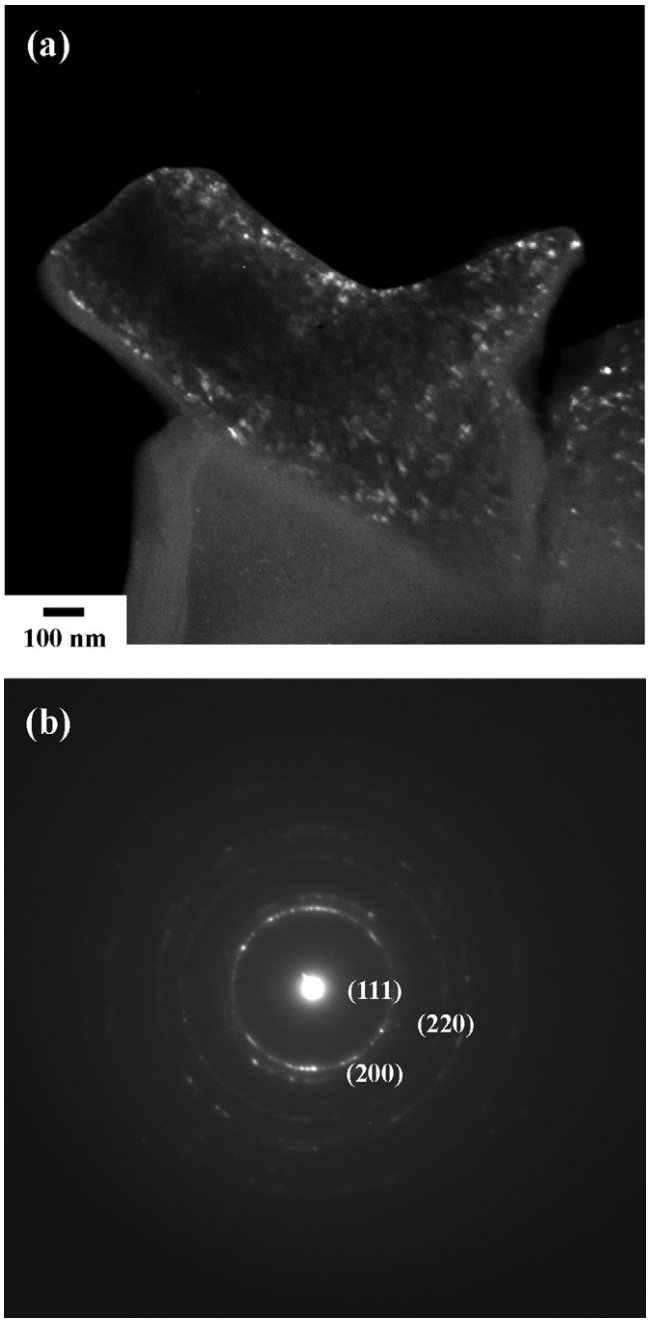

Fig. 6. (a) TEM dark field image of the reaction product layer in the Al/HEA interface, and (b) SAD pattern showing the reaction product layer was composed of the FCC nanocrystalline structure.

micrograph demonstrated in Fig. 6(a) shows that many tiny particles smaller than 10 nm are found dispersed in an amorphous matrix. The SAD pattern depicted in Fig. 6(b) confirms the FCC nanocrystalline structure nature of the bright particle existing in the NPL layer.

3.2. Solidified Al melt

Fig. 7(a) shows the SEM micrograph in BSE mode of the solidified pure Al melt without HEA dipping. Other than polishing scratches and a few shrinkage voids, no precipitates or distinct phases can be seen in Fig. 7(a), indicating a homogeneous microstructure. With the dipping of HEA into the Al melt, the dissolution of the alloying elements from the HEA modifies the chemical composition of the

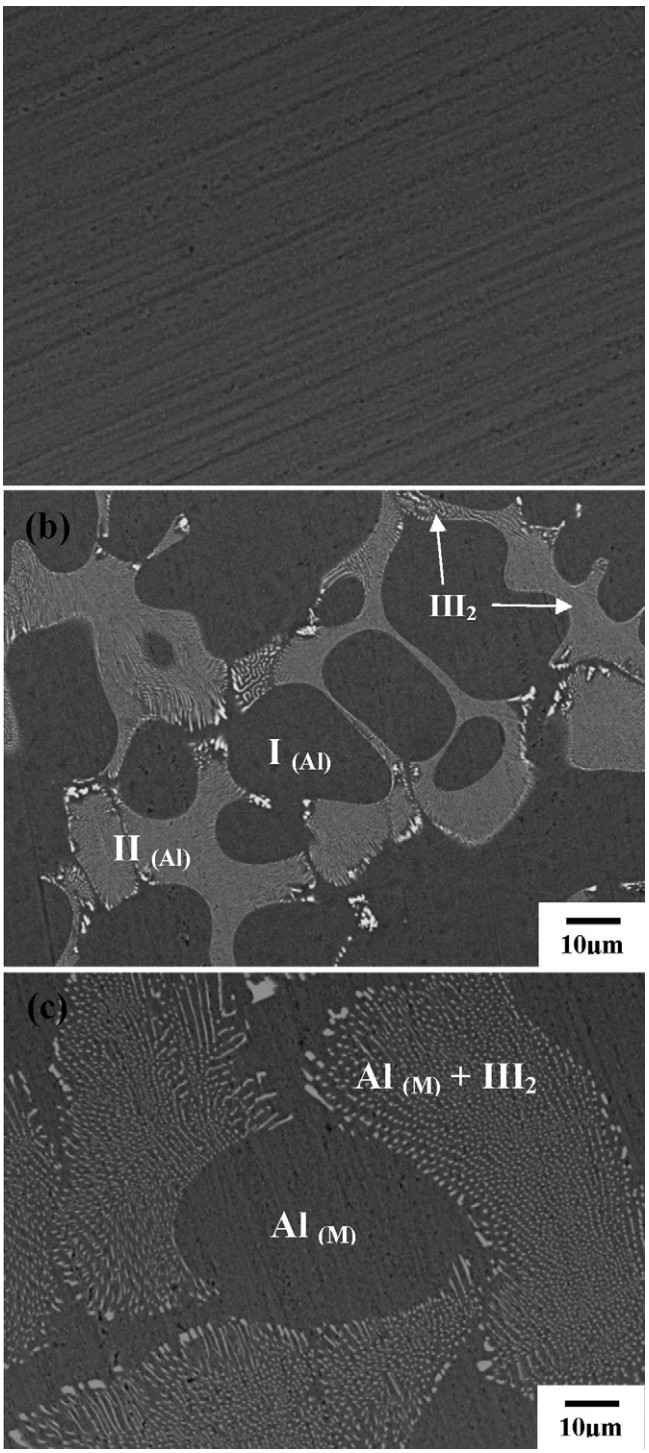

Fig. 7. Magnified cross-section BSE images of solidified Al melt after holding at 700 °C, (a) the solidified pure Al melt without HEA immersion, (b) the solidified Al melt with HEA immersion and (c) the solidified Al melt with HEA immersion remained in alumina crucible where the $Al_{(M)}$ and eutectic structure is formed.

Al melt and causes a change in the microstructure of the solidified melt. The SEM micrograph depicting the microstructure of the Al melt after HEA immersion for 1 h is shown in Fig. 7(b). This micrograph reveals the multi-phase and complicated microstructure of the solidified melt. The alloying elements dissolved from the HEA modify the chemical composition of the Al liquid phase. EDS analysis shows that the grey area (region $I_{(Al)}$ in Fig. 7(b)) contains relatively higher amounts of Fe, Ni and Co. A lamellar

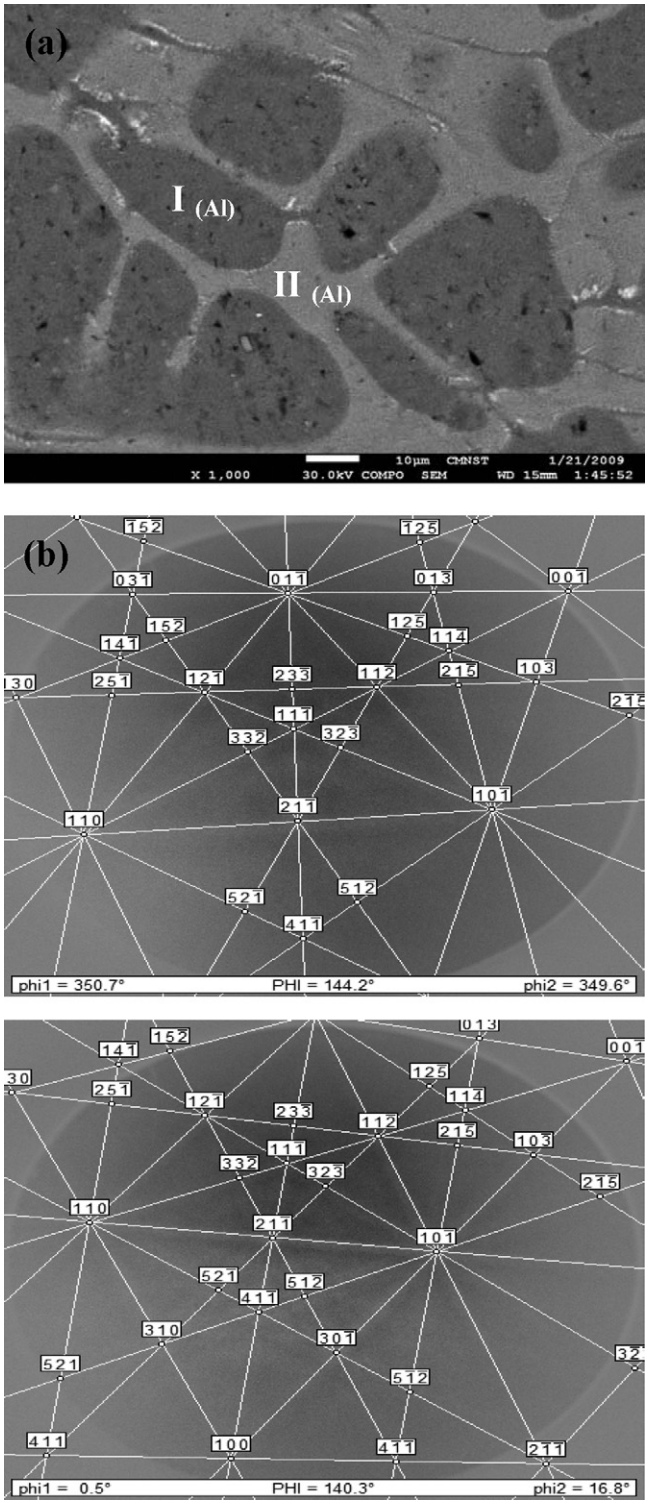

Fig. 8. (a) The eutectic structure in the solidified Al melt obtained from SEM, and the EBSD Kikuchi pattern of (b) region $I_{(Al)}$, and (c) region $II_{(Al)}$ as shown in (a).

microstructure (marked as region $II_{(Al)}$ in Fig. 7(b)) exhibiting the eutectic characteristics of the image are also revealed in this micrograph. The white platelet (designated as III_2 phase) contains less amounts of Fe, Ni and Co as compared with those of the grey phase. Since the solubility of Fe, Ni and Co in the Al liquid phase are much higher than in the solid phase [16], therefore, phase change and chemical composition segregation occurs when the liquid phase is cooled to room temperature. The high volume fraction of eutectic microstructure was noted in Fig. 7(b) indicates that great amounts of transition metal elements are dissolved from the HEA into the Al melt. Furthermore, the existence of the eutectic microstructure in the solidified Al remaining in the crucible can also be observed (see Fig. 7(c)), indicating the fact that the diffusion rate of each transition metal atom dissolved in the Al liquid phase is very fast.

The phase change in the outer solidified Al melt was also analyzed by EBSD. The SEM image and the Kikuchi pattern shown in Fig. 8 represent those with HEA hot dipping for 1 h. The dark region ($I_{(Al)}$) shown in Fig. 8(a) is the primary solidified phase which contains a relatively high amount of Fe, Ni and Co, while region $II_{(Al)}$ consists of two phases with lamellar microstructure and very fine size platelets. The Kikuchi pattern representing region $I_{(Al)}$ shown in Fig. 8(a) is displayed in Fig. 8(b). This pattern corresponds to the FCC crystal structure of the phase in region $I_{(Al)}$. The Kikuchi pattern of region $II_{(Al)}$ displayed in Fig. 8(c) also exhibits the characteristics of FCC crystal structure, even though it consists of two phases with different chemical compositions. Since the Kikuchi pattern only displays single crystal structure characteristics, the two phases present in the eutectic microstructure should have the same crystal structure.

4. Conclusions

When the FeCrNiCoMnAl high entropy alloy comes into contact with Al melt, a complicated reaction takes place at the interface and significant changes in chemical composition and microstructure in the solid substrate and the solidified Al melt are observed.

The dissolution of Al into the HEA can cause a lowering of the melting point of phase II much greater than that of phase I. As a result, a higher rate of retreat in the solid phase at the II/Al interface as compared with that at the I/Al interface is observed. The dipping of HEA into the molten aluminum leads to a significant change in chemical composition both in the substrate and the Al melt. The formation of a FCC nanocrystalline layer immediately above the HEA is observed, as identified by EBSD and TEM. Beyond that, some large particles containing high concentration of Cr are found. In the solidified Al melt, the dissolution of the transition metal elements causes both the precipitation of new phases and chemical composition segregation in the solidified Al crust. A lamellar microstructure exhibiting eutectic characteristics is found. The Kikuchi pattern obtained from EBSD analysis only displays single crystal structure characteristics. The new phases formed in the initial Al melt all exhibit FCC crystal structure, though they have different chemical compositions.

Acknowledgements

The authors would like to thank Industrial Technology Research Institute for supporting this work. The partial support of National Science Council of the Republic of China under Contract NSC 98-2221-E-006-067-MY3 for the use of instruments for material characterization is also acknowledged.

References

[1] H.R. Shahverdi, M.R. Ghomashchi, S. Shabestari, J. Hejazi, J. Mater. Proc. Technol. 124 (2002) 345–352.
[2] Y. Zhu, D. Schwam, J.F. Wallace, S. Birceanu, Int. J. Mater. Sci. Eng. A 379 (2004) 420–431.
[3] J.C. Viala, M. Peronnet, F. Barbeau, F. Bosselet, J. Bouix, Appl. Sci. Manuf. 33 (2002) 1417–1420.
[4] D. Wang, Z. Shi, L. Zou, Appl. Surf. Sci. 214 (2003) 304–311.
[5] A. Persson, J. Bergstrom, C. Burman, S. Hogmark, Surf. Coat. Technol. 146–147 (2001) 42–47.
[6] J.W. Yeh, S.K. Chen, S.J. Lin, J.Y. Gan, T.S. Chin, T.T. Shun, C.H. Tsau, S.Y. Chang, Adv. Eng. Mater. 6 (2004) 299–303.
[7] J.W. Yeh, S.K. Chen, J.Y. Gan, S.U. Lin, T.S. Chin, T.T. Shun, C.H. Tsau, S.Y. Chang, Metall. Mater. Trans. A 35 (2004) 2533–2536.

[8] C.J. Tong, Y.L. Chen, S.W. Chen, J.W. Yeh, T.T. Shun, C.H. Tsau, S.J. Lin, S.Y. Chang, Metall. Mater. Trans. A 36A (2005) 881–893.
[9] Y.J. Zhou, Y. Zhang, Y.L. Wang, G.L. Chen, Mater. Sci. Eng. A 454–455 (2007) 260–265.
[10] C.Y. Hsu, J.W. Yeh, S.K. Chen, T.T. Shun, Metall. Mater. Trans. A 35 (2004) 1465–1469.
[11] P.K. Huang, J.W. Yeh, T.T. Shun, S.K. Chen, Adv. Eng. Mater. 6 (2004) 74–78.
[12] Y.S. Huang, L. Chen, H.W. Lui, M.H. Cai, J.W. Yeh, Mater. Sci. Eng. A 457 (2007) 77–83.
[13] C.J. Tong, M.R. Chen, S.K. Chen, J.W. Yeh, T.T. Shun, S.J. Lin, S.Y. Chang, Met. Mater. Trans. A. 36 (2005) 1265–1271.
[14] Y. Zhang, G.L. Chen, L. Gan, J. ASTM Int. 7 (2010) JAI102527.
[15] G.M. William, The Handbook of Binary Phase Diagrams, Geniurn Pub, Schenectady, New York, 1990.
[16] E.M. Dunn, in: J.E. Hatch (Ed.), Aluminum Properties and Physical Metallurgy, American Society for Materials, Materials Park, Ohio, 1984, pp. 26–27.